Distributed Collaborative Beamforming Designs for Real-World Applications in Relayed and Cooperative Communications

(Invited Paper)

Slim Zaidi and Sofiène Affes

INRS-EMT, 800, de la Gauchetière Ouest, Bureau 6900, Montréal, H5A 1K6, Qc, Canada,

Email: {zaidi,affes}@emt.inrs.ca

Abstract—Three main distributed collaborative beamforming (DCB) designs based on different channel models could be employed in real-world applications where scattering and implementation imperfections might exist: the monochromatic (i.e., single-ray) DCB (M-DCB), the bichromatic (i.e., two-ray) DCB (B-DCB), and the polychormatic (i.e., multi-ray) DCB (P-DCB). In this paper, we perform an analytical comparison, under practical constraints, between these DCB designs in terms of achieved signal-to-noise ratio (SNR) as well as achieved throughput. Assuming the presence of scattering and accounting for implementation errors incurred by each DCB design, we derive closed-form expressions of their true achieved SNRs. Excluding exceptional circumstances of unrealistic low quantization levels (i.e., very large quantization errors) hard to justify in practice, we show that B-DCB always outperforms M-DCB as recently found nominally in ideal conditions. We also show that for low AS B-DCB and P-DCB achieve almost the same SNR while for high AS the latter outperforms the first. Furthermore, this work pushes the performance analysis of DCB to the throughput level by taking into account the feedback overhead cost incurred by each design. We prove both by concordant analysis and simulations that the P-DCB's throughput gain against B-DCB reduces as the channel Doppler frequency increases.

I. Introduction and Background

Collaborative beamforming (CB) is a strong means to establish energy-efficient and reliable communications over long distances [1]-[12]. Despite of its practical merits, CB faces an important issue. Indeed, the collaborating terminals are very often autonomous small battery-powered units which have limited knowledge about each other in the network. In the very likely event where the beamforming weights would depend on the locally unavailable information at every terminal, the latter would not be able to compute its own weight without severely depleting power and bandwidth due to the potentially huge information exchange requested [11]. Lending themselves to a distributed implementation, a variety of so-called distributed CB (DCB) techniques wherein the designed weights solely depend on the information commonly available at every terminal and, hence, each terminal is able to locally compute its own weight were proposed in [11] and [12]. Until recently, however, such works neglected the scattering and reflection effects and assumed plane-wave (single-ray)

propagation channels termed here as monochromatic (with reference to their angular distribution). This assumption is not valid in real-world environments where the presence of local scattering in the source vicinity causes an angular spread (AS) of the transmit signal that forms a multi-ray propagation channel [13]-[19], termed her as polychromatic. Due to the resulting mismatch between the nominal monochromatic and the true polychromatic channels, it was shown in [14] that the performance of monochromatic DCB (M-DCB) techniques degrades in rural areas where the AS is still very small and becomes unsatisfactory when the AS increases such as in suburban and urban areas. This impediment unfortunately limits the DCB's real-world applicability range. Exploiting an efficient two-ray approximation of the polychromatic channel at relatively low AS, we have recently developed in [17] and [18] a new bichromatic (i.e., two-ray) DCB (B-DCB) design which achieves optimal performance for low AS such as in rural and suburban areas. Aiming to further push the DCB's real-world applicability, a polychromatic (i.e., multi-ray) DCB (P-DCB) has been very recently proposed in [19]. This design which avoids the two-ray approximation and, hence, accounts for the true polychromatic nature of the channel, turns out to be able to achieve optimal performance even in urban areas.

This work provides a performance analysis and comparison under real-world conditions of the aforementioned DCB designs. We derive their true achieved SNRs in closed-form taking into account estimation and feedback quantization errors. Excluding exceptional circumstances of unrealistic low quantization levels (i.e., very large quantization errors) hard to justify in practice, we show that B-DCB always outperforms M-DCB as recently found nominally in ideal conditions. We also show that for low AS B-DCB and P-DCB achieve almost the same SNR while for high AS the latter outperforms the first. Furthermore, this work pushes the performance analysis of DCB to the throughput level by taking into account the feedback overhead cost incurred by each design. We prove both by concordant analysis and simulations that the P-DCB's throughput gain against B-DCB reduces as the channel Doppler frequency increases.

The rest of this paper is organized as follows. The system model is described in Section II. The DCB designs are introduced in Section III. Section IV compares the performance of
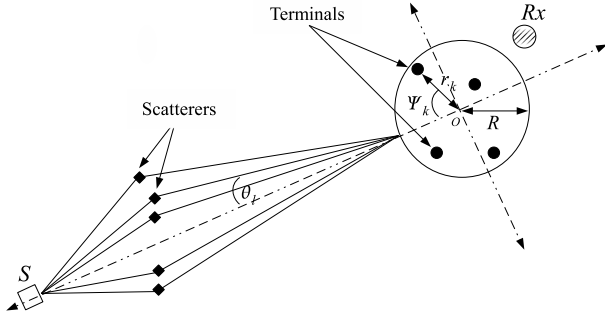
Fig. 1. System model.

these techniques in terms of ASANR while Section V compares them in terms of the link-level throughput. Simulations results are shown in Section VI and concluding remarks are given in Section VII.

Notation: Uppercase and lowercase bold letters denote matrices and vectors, respectively. $[\cdot]_{il}$ and $[\cdot]_i$ are the (i,l)-th entry of a matrix and i-th entry of a vector, respectively. $\mathbf{I}$ is the identity matrix and $\mathbf{e}_l$ is a vector with one in the l-th position and zeros elsewhere. $(\cdot)^T$ and $(\cdot)^H$ denote the transpose and the Hermitian transpose, respectively. $\|\cdot\|$ is the 2-norm of a vector and $|\cdot|$ is the absolute value. $E\{\cdot\}$ stands for the statistical expectation and $(\xrightarrow{ep1})$ $\xrightarrow{p1}$ denotes (element-wise) convergence with probability one. $J_1(\cdot)$ is the first order Bessel function of the first kind and $\odot$ is the element-wise product.

II. SYSTEM MODEL

As illustrated in Fig. 1, the system of interest consists of a wireless network or subnetwork comprised of K uniformly and independently distributed terminals on $D(O,R)$, the disc with center at O and radius R, a receiver at O, and a source S located in the same plane containing $D(O,R)$ [9], [10]. We assume that there is no direct link from the source to the receiver due to pathloss attenuation. Moreover, let (r_k, ψ_k) denote the polar coordinates of the k-th terminal and (A_s, ϕ_s) denote those of the source. The latter is assumed to be at $\phi_s = 0$, without loss of the generality, and to be located in the far-field region, hence, $A_s \gg R$.

The following assumptions are further considered:

A1) The far-field source is scattered by a large number of scatterers within its vicinity. The latters generate from the transmit signal L equal-power rays or "spatial chromatics" (with reference to their angular distribution) that form an L-ray propagation channel [13]-[16]. The l-th ray or chromatic is characterized by its angle θ_l and its complex amplitude $\alpha_l = \rho_l e^{j\xi_l}$ where the amplitudes ρ_l, $l = 1, \ldots, L$ and the phases ξ_l, $l = 1, \ldots, L$ are independent and identically distributed (i.i.d.) random variables, and each phase is uniformly distributed over $[-\pi, \pi]$. The θ_l, $l = 1, \ldots, L$ are also i.i.d. random variables with variance σ_θ^2 and probability density function (pdf) $p(\theta)$ [13]-[16]. All θ_ls, ξ_ls, and ρ_ls are mutually independent. Note that the standard deviation σ_θ is commonly known as the angular spread (AS) while $p(\theta)$ is called the scattering or angular distribution.

A2) The channel gain $[\mathbf{f}]_k$ between the k-th terminal and the receiver is a zero-mean unit-variance circular Gaussian random variable [11]. The source signal s is a zero-mean random variable with unit-power while noises at terminals and the receiver are zero-mean Gaussian random variables with variances $\sigma_v{}^2$ and $\sigma_n{}^2$, respectively. The source signal, noises, and the terminals forward or backward channel gains are mutually independent [11].

A4) The k-th terminal is aware of its own coordinates (r_k, ψ_k), its forward channel $[\mathbf{f}]_k$, the directions of the source ϕ_s, K, and σ_θ^2 while being oblivious to the locations and the forward and backward channels of *all* other terminals in the network.

Using A1 and the fact that $A_s \gg R$, the channel gain between the k-th terminal and the source or the receiver, respectively, can be represented as $[\mathbf{g}]_k = \sum_{l=1}^{L} \alpha_l e^{-j\frac{2\pi}{\lambda} r_k \cos(\theta_l - \psi_k)}$ where λ is the wavelength.

A dua-hop communication is established from the source S to the receiver. In the first time slot, the source sends its signal s to the wireless network. Let $\mathbf{y}$ denotes the received signal vector at the terminals given by

$$\mathbf{y} = \mathbf{g}s + \mathbf{v}, \tag{1}$$

where $\mathbf{v}$ is the terminals' noise vector. In the second time slot, the k-th terminal multiplies its received signal with the complex conjugate of the beamforming weight w_k and forwards the resulting signal to the receiver. It follows from (1) that the received signal at O is

$$
\begin{aligned}
r &= \mathbf{f}^T (\mathbf{w}^* \odot \mathbf{y}) + n = \mathbf{w}^H (\mathbf{f} \odot \mathbf{y}) + n \\
&= \mathbf{w}^H (\mathbf{f} \odot \mathbf{g}s + \mathbf{f} \odot \mathbf{v}) + n \\
&= s\mathbf{w}^H \mathbf{h} + \mathbf{w}^H (\mathbf{f} \odot \mathbf{v}) + n,
\end{aligned} \tag{2}
$$

where $\mathbf{w} \triangleq [w_1 \ldots w_K]$ is the beamforming vector, $\mathbf{h} \triangleq \mathbf{f} \odot \mathbf{g}$, $\mathbf{f} \triangleq [[\mathbf{f}]_1 \ldots [\mathbf{f}]_K]^T$, and n is the receiver noise. Several approaches can be adopted to properly select the beamforming weights. In this paper, we are only concerned with the approach that aims to minimize the noise power while fixing the beamforming response in the desired direction at a certain level considered here, for simplicity, equal to 1. Mathematically, we have to solve the following optimization problem:

$$\mathbf{w}_O = \arg\min \mathbf{w}^H \mathbf{\Lambda} \mathbf{w} \qquad \text{s.t.} \qquad \mathbf{w}^H \mathbf{h} = 1, \tag{3}$$

where $\mathbf{w}_O$ is the optimal CB (OCB)'s beamforming vector, $\mathbf{\Lambda} \triangleq \text{diag}\{|[\mathbf{f}]_1|^2 \ldots |[\mathbf{f}]_K|^2\}$. It can be readily proven that $\mathbf{w}_O$ is given by

$$\mathbf{w}_O = \left(\mathbf{h}_O^H \mathbf{\Lambda}^{-1} \mathbf{h}_O\right)^{-1} \mathbf{\Lambda}^{-1} \mathbf{h} \tag{4}$$

A straightforward inspection of (4) reveals that $\mathbf{w}_O$ depends on information locally-unavailable at every node making the OCB a non-distributed solution [20], [21]. In what follows, we introduce the main DCB designs in the literature and compare their performances, in real-world environments, with one another and also with the non-distributed optimal design in (4).

III. Distributed collaborative beamforming (DCB) designs

In this section, we focus on there main DCB designs: the monochromatic (i.e., single-ray) DCB (M-DCB), the bichromatic (i.e., two-ray) DCB (B-DCB), and the polychromatic (i.e., multi-ray) DCB (P-DCB).

A. M-DCB design

This design, which has been the sole truly-distributed design for almost a decade, intentionally neglects the scattering effect (i.e., assume that $\sigma_\theta \to 0$) to nominally assume a monochromatic single-ray propagation channels and, hence, the beamforming vector associated with M-DCB is given by [9]

$$\mathbf{w}_{\mathrm{M}} = \mu_{\mathrm{M}} \mathbf{\Lambda}^{-1} \mathbf{h}_{\mathrm{M}}, \tag{5}$$

where $\mathbf{h}_{\mathrm{M}} = \mathbf{a}(0)$ with $[\mathbf{a}(\theta)]_k = [\mathbf{f}]_k e^{-j(2\pi/\lambda)r_k \cos(\theta + \phi_s - \psi_k)}$ and $\mu_{\mathrm{M}} = \left(\mathbf{a}(0)^H \mathbf{\Lambda}^{-1} \mathbf{a}(0)\right)^{-1} = 1/K$. Also known as conventional DCB, this beamformer implementation requires that the source estimates, quantizes and sends only its direction ϕ_s [9]. This process results in both localization and quantization errors and, hence, the channel $\mathbf{h}_{\mathrm{M}}$ should be substituted by $\hat{\mathbf{h}}_{\mathrm{M}} = \mathbf{h}_{\mathrm{M}} e^{-j(\mathbf{e}_a + \mathbf{e}_{aq})}$ where $\mathbf{e}_a$ and $\mathbf{e}_{aq}$ are the angle localization and quantization errors, respectively. Assuming that these errors are relatively small and using Taylor's series series expansion, one can easily prove that $\hat{\mathbf{h}}_{\mathrm{M}} \simeq \mathbf{h}_{\mathrm{M}} + \mathbf{e}_{\mathrm{M}}$ where $\mathbf{e}_{\mathrm{M}} = -j\mathbf{h}_{\mathrm{M}}(\mathbf{e}_a + \mathbf{e}_{aq})$ with variance $\sigma^2_{\mathbf{e}_{\mathrm{M}}} = \sigma^2_{\mathbf{e}_a} + \sigma^2_{\mathbf{e}_{aq}}$. Using a $(B_a + 1)$-bit uniform quantization, it can be shown that $\sigma^2_{\mathbf{e}_{aq}} = 2^{-2B_a}\frac{4\pi^2}{12}$ [23]. In turn, we use the CRLB developed in [24] to define $\sigma^2_{\mathbf{e}_a}$ and, hence, $\sigma^2_{\mathbf{e}_a} = \frac{4\sin^2\left(\frac{\pi}{K}\right)\sigma^2_v}{NK\pi^2}$ where N is the number of samples using to estimate ϕ_s. Taking into account the aforementioned consideration, the practical M-DCB beamforming vector is now given by

$$\hat{\mathbf{w}}_{\mathrm{M}} = \hat{\mu}_{\mathrm{M}} \mathbf{\Lambda}^{-1} \hat{\mathbf{h}}_{\mathrm{M}}, \tag{6}$$

where $\hat{\mu}_{\mathrm{M}} = \left(\hat{\mathbf{h}}_{\mathrm{M}}^H \mathbf{\Lambda}^{-1} \hat{\mathbf{h}}_{\mathrm{M}}\right)^{-1}$.

B. B-DCB design

Exploiting the fact that for low AS a multi-ray channel - owing to a Taylor series expansion of its correlation matrix- can be properly approximated by two angular rays and hence considered as bichromatic, a bichromatic distributed CB (B-DCB) was recently proposed in [17] and [18]. Its beamforming vector is given by

$$\mathbf{w}_{\mathrm{B}} = \mu_{\mathrm{B}} \mathbf{\Lambda}^{-1} \mathbf{h}_{\mathrm{B}}, \tag{7}$$

where $\mathbf{h}_{\mathrm{B}} = \frac{1}{2}\left(\mathbf{a}(\sigma_\theta) + \mathbf{a}(-\sigma_\theta)\right)$ and $\mu_{\mathrm{B}} = \frac{2}{K}\left(1 + 2\frac{J_1(\gamma(2\sigma_\theta))}{\gamma(2\sigma_\theta)}\right)^{-1}$. Note that in the conventional scenario where the local scattering effect is neglected (i.e., $\sigma_\theta \to 0$) to assume monochromatic propagation channels, (7) is reduced to (5). It is also noteworthy that the B-DCB's implementation requires that the source estimates, quantizes and sends its direction ϕ_s and the AS σ_θ, thereby resulting

in both estimation and quantization errors. The channel $\mathbf{h}_{\mathrm{B}}$ should be then substituted by $\hat{\mathbf{h}}_{\mathrm{B}} = \mathbf{h}_{\mathrm{B}} e^{-j(\mathbf{e}_a + \mathbf{e}_{aq} + \mathbf{e}_s + \mathbf{e}_{sq})}$ where $\mathbf{e}_s$ and $\mathbf{e}_{sq}$ are the AS estimation and quantization errors, respectively. Using the same approach as above, one can easily show for relatively small errors that $\hat{\mathbf{h}}_{\mathrm{B}} = \mathbf{h}_{\mathrm{B}} + \mathbf{e}_{\mathrm{B}}$ where $\mathbf{e}_{\mathrm{B}} = -j\mathbf{h}_{\mathrm{B}}(\mathbf{e}_a + \mathbf{e}_{aq} + \mathbf{e}_s + \mathbf{e}_{sq})$ with variance $\sigma^2_{\mathbf{e}_{\mathrm{B}}} = \sigma^2_{\mathbf{e}_a} + \sigma^2_{\mathbf{e}_{aq}} + \sigma^2_{\mathbf{e}_s} + \sigma^2_{\mathbf{e}_{sq}}$. Using a $(B_s + 1)$-bit uniform quantization, it can be shown that $\sigma^2_{\mathbf{e}_{sq}} = 2^{-2B_s}\frac{\pi^2}{12}$ [23]. Since AS estimation can be modeled as a DoA estimation of two point sources, we also use for simplicity the CRLB developed in [24] to define $\sigma^2_{\mathbf{e}_s}$ and, hence, $\sigma^2_{\mathbf{e}_s} = \sigma^2_{\mathbf{e}_a}$. Therefore, the B-DCB beamforming weight is now

$$\hat{\mathbf{w}}_{\mathrm{B}} = \hat{\mu}_{\mathrm{B}} \mathbf{\Lambda}^{-1} \hat{\mathbf{h}}_{\mathrm{B}}, \tag{8}$$

where $\hat{\mu}_{\mathrm{B}} = \frac{2}{K}(1 + \sigma^2_{\mathbf{e}_{\mathrm{B}}})^{-1}\left(1 + 2\frac{J_1(\gamma(2\sigma_\theta))}{\gamma(2\sigma_\theta)}\right)^{-1}$.

C. P-DCB design

P-DCB design relies on an efficient approximation at large K of the OCB weights. Its beamforming vector is given by [19]

$$\mathbf{w}_{\mathrm{P}} = \mu_{\mathrm{P}} \mathbf{\Lambda}^{-1} \mathbf{h}_{\mathrm{P}} \tag{9}$$

where $\mu_{\mathrm{P}} = \frac{1}{K}\left(\sum_{l=1}^{L}\sum_{m=1}^{L} \alpha_l \alpha_m^* \Delta(\theta_l - \theta_m)\right)^{-1}$, $\Delta(\phi) = J_1\left(4\pi\frac{R}{\lambda}\sin(\phi/2)\right)/4\pi\frac{R}{\lambda}\sin(\phi/2)$, and $\mathbf{h}_{\mathrm{P}} = \mathbf{h}$. From (9), in order to implement the P-DCB technique, the source must estimate and quantize the channels $[\mathbf{h}]_k, k = 1\ldots K$ before sending them back to all K terminals. This process unfortunately results in both estimation and quantization errors as well as an important overhead. Let us denote the resulting channel vector by $\hat{\mathbf{h}}_{\mathrm{P}} = \mathbf{h}_{\mathrm{P}} + \mathbf{e}_{\mathrm{P}}$ where $\mathbf{e}_{\mathrm{P}} = \mathbf{f} \odot \mathbf{e}_c + \mathbf{f} \odot \mathbf{e}_{cq}$ and $\mathbf{e}_c$ and $\mathbf{e}_{cq}$ are the channel identification and quantization errors, respectively. Let us denote the variance of $\mathbf{e}_{\mathrm{O}}$ by $\sigma^2_{\mathbf{e}_{\mathrm{O}}} = \sigma^2_{\mathbf{e}_c} + \sigma^2_{\mathbf{e}_{cq}}$ where $\sigma^2_{\mathbf{e}_c}$ and $\sigma^2_{\mathbf{e}_{cq}}$ are the variances of $\mathbf{e}_c$ and $\mathbf{e}_{cq}$, respectively. We can show that $\sigma^2_{\mathbf{e}_c} = \frac{3K}{2}\left(\pi\sigma^2_v \bar{f}_{\mathrm{D}}\right)^{\frac{2}{3}}$ where $\bar{f}_{\mathrm{D}}$ is the normalized Doppler frequency [22]. Moreover, assuming a $(B_c + 1)$-bit uniform quantization we have $\sigma^2_{\mathbf{e}_{cq}} = 2^{-2B_c}\frac{h^2_{\mathrm{Max}}}{12}$ where h_{Max} is the peak amplitude of all channels' realizations $[\mathbf{h}]_k$ for $k = 1,\ldots,K$ [23]. Taking into account these considerations, the Ps beamforming vector is now given by

$$\hat{\mathbf{w}}_{\mathrm{P}} = \hat{\mu}_{\mathrm{P}} \mathbf{\Lambda}^{-1} \hat{\mathbf{h}}_{\mathrm{P}} \tag{10}$$

where $\hat{\mu}_{\mathrm{P}} = \frac{1}{K}(1 + \sigma^2_{\mathbf{e}_{\mathrm{P}}})^{-1}\left(\sum_{l=1}^{L}\sum_{m=1}^{L} \alpha_l \alpha_m^* \Delta(\theta_l - \theta_m)\right)^{-1}$.

IV. Performance analysis in terms of ASANR

In order to analyze and compare the DCB designs' performances, we introduce the following performance measure:

$$\tilde{\Upsilon}_\star(\sigma_\theta) = \frac{\tilde{\xi}_{\hat{\mathbf{w}}_\star}}{\tilde{\xi}_{\hat{\mathbf{w}}_{\mathrm{B}}}}, \tag{11}$$

where $\tilde{\xi}_{\mathbf{w}} = \tilde{P}_{\mathbf{w}}(\phi_s)/\tilde{P}_{\mathbf{w},n}$ is the achieved average-signal-to-average-noise ratio (ASANR) when $\mathbf{w}$ is implemented with $\tilde{P}_{\mathbf{w}}(\phi_\star) = \mathrm{E}\left\{|\mathbf{w}^H \mathbf{h}|^2\right\}$, called the average beampattern, and $\tilde{P}_{\mathbf{w},n} = \sigma^2_v \mathrm{E}\left\{\mathbf{w}^H \mathbf{\Lambda} \mathbf{w}\right\} + \sigma^2_n$ is the average noise power.

Note that it is also interesting to study the behavior of a more practical performance measure, the average SNR (ASNR) $\bar{\xi}_{\mathbf{w}} = \mathrm{E}\{P_{\mathbf{w}}(\phi_s)/P_{\mathbf{w},n}\}$ where the expectation is taken with respect to the random variables r_k, ψ_k and $[\mathbf{f}]_k$ for $k = 1, \ldots, K$ and α_l and θ_l for $l = 1, \ldots, L$. Since $P_{\mathbf{w}}(\phi_s)$ and $P_{\mathbf{w},n}$ are very complicated functions of the latter random variables, deriving a closed-form expression for $\bar{\xi}_{\mathbf{w}}$ appears, however, to be extremely difficult if not impossible. This also suggests that it is more practical to analyze the behavior of the achieved ASANR. Furthermore, it has been in [18] that the achieved ASANR and ASNR using any $\mathbf{w} \in \{\mathbf{w}_{\mathrm{M}}, \mathbf{w}_{\mathrm{B}}, \mathbf{w}_{\mathrm{P}}\}$ have the same asymptotic behaviors when K grows large. This further motivates us to analyze and compare ASANRs achieved by the B-DCB design

Using the fact that $\mathbf{h}$ and $\mathbf{e}_\star$ are statistically independent, $\tilde{\xi}_{\hat{\mathbf{w}}_\star}$ can then be expressed as

$$\tilde{\xi}_{\hat{\mathbf{w}}_\star} = \frac{\tilde{P}_{\mathbf{w}_\star}(\phi_s) + \mathrm{E}\left\{\mu_\star^2 \|\mathbf{h}^H \mathbf{\Lambda}^{-1} \mathbf{e}_\star\|^2\right\}}{\tilde{P}_{\mathbf{w}_\star,n} + \sigma_v^2 \mathrm{E}\{\mu_\star^2 \mathbf{e}_\star^H \mathbf{\Lambda}^{-1} \mathbf{e}_\star\} + \sigma_n^2 \left(\mathrm{E}\left\{\left(\frac{\mu_\star}{\hat{\mu}_\star}\right)^2\right\} - 1\right)}. \quad (12)$$

Note that the each of the numerator and denominator decomposes into two terms corresponding to channel mismatch contribution (i.e., $\tilde{P}_{\mathbf{w}_\star}(\phi_s)$ or $\tilde{P}^{\mathrm{r}}_{\mathbf{w}_\star,n}$, respectively) and channel quantization/estimation errors contribution (i.e., each remainder).

A. ASANR of M-DCB vs. B-DCB

Using the results in [17] and [18], it can be shown for large K that

$$\tilde{\Upsilon}_{\mathrm{M}}(\sigma_\theta) = \tilde{\Upsilon}_{\mathrm{M}}^{\mathrm{IDL}}(\sigma_\theta)\left(\frac{1 + \sigma_{\mathbf{e}_{\mathrm{B}}}^2}{1 + \sigma_{\mathbf{e}_{\mathrm{M}}}^2}\right)^2, \quad (13)$$

where $\tilde{\Upsilon}_{\mathrm{M}}^{\mathrm{IDL}}(\sigma_\theta) = \Gamma(0)\left(1 + 2\frac{J_1(\gamma(2\sigma_\theta))}{\gamma(2\sigma_\theta)}\right)^2/4\Omega(0)$ with $\Omega(\phi) = \int p(\theta)\left(\frac{J_1(\gamma(\phi+\theta+\sigma_\theta))}{\gamma(\phi+\theta+\sigma_\theta)} + \frac{J_1(\gamma(\phi+\theta-\sigma_\theta))}{\gamma(\phi+\theta-\sigma_\theta)}\right)^2 d\theta$ and $\Gamma(\phi) = \int p(\theta)\left(2\frac{J_1(\gamma(\phi+\theta))}{\gamma(\phi+\theta)}\right)^2 d\theta$. $\tilde{\Upsilon}_\star^{\mathrm{IDL}}(\sigma_\theta)$ refers actually to the ASANR gain of $\mathbf{w}_\star$ against $\mathbf{w}_{\mathrm{B}}$ achieved in ideal conditions where all the estimation and quantization errors are negligible. In [18], we proved that $\tilde{\Upsilon}_{\mathrm{M}}^{\mathrm{IDL}}(\sigma_\theta) \leq 1$ and the ASANR gain achieved using $\mathbf{w}_{\mathrm{B}}$ instead of $\mathbf{w}_{\mathrm{M}}$ can reach as much as 3 dB for high AS. However, from (13), $\tilde{\Upsilon}_{\mathrm{M}}(\sigma_\theta) < \tilde{\Upsilon}_{\mathrm{M}}^{\mathrm{IDL}}(\sigma_\theta)$ only when $\sigma_{\mathbf{e}_{\mathrm{B}}}^2 > \sigma_{\mathbf{e}_{\mathrm{M}}}^2$ (i.e., small B_{a} and B_{s}). Therefore, the B-DCB always outperforms the M-DCB as found in ideal conditions, excluding exceptional circumstances of unrealistic low quantization levels (i.e., very large quantization errors) hard to justify in practice.

B. ASANR of B-DCB vs. P-DCB

In this section we carry out a comparison between the B-DCB and its P-DCB vis-a-vis. It can be shown that $\tilde{\Upsilon}_{\mathrm{P}}$ is given by [18] [19]

$$\tilde{\Upsilon}_{\mathrm{P}}(\sigma_\theta) = \tilde{\Upsilon}_{\mathrm{P}}^{\mathrm{IDL}}(\sigma_\theta) \frac{(1 + \sigma_{\mathbf{e}_{\mathrm{B}}}^2)^2}{1 + 2\frac{\sigma_{\mathbf{e}_{\mathrm{P}}}^2 L}{L-1} + \frac{\sigma_{\mathbf{e}_{\mathrm{P}}}^4 L^2}{(L-1)(L-2)}}, \quad (14)$$

where $\tilde{\Upsilon}_{\mathrm{P}}^{\mathrm{IDL}}(\sigma_\theta) = \left(\left(1 + 2\frac{J_1(\gamma(2\sigma_\theta))}{\gamma(2\sigma_\theta)}\right)^2\right)/4\Omega(0)$. From the latter definition, we have $\tilde{\Upsilon}_{\mathrm{P}}^{\mathrm{IDL}}(0) = 1$. This is expected since, when there is no local scattering in the source vicinity (i.e., $\sigma_\theta = 0$), $\mathbf{w}_{\mathrm{P}} = \mathbf{w}_{\mathrm{B}}$. Simulations results in Section VI will show that $\tilde{\Upsilon}_{\mathrm{P}}^{\mathrm{IDL}}(\sigma_\theta) = 1$ also holds, in rural and suburban areas where $\sigma_\theta \neq 0$ but relatively small. However, when σ_θ is relatively large such as in urban areas, one can easily show that $J_1(\gamma(2\sigma_\theta))/\gamma(2\sigma_\theta) \simeq 0$ [11] and, hence, $\tilde{\Upsilon}_{\mathrm{P}}^{\mathrm{IDL}}(\sigma_\theta) \simeq (4\Omega(0))^{-1}$. Since $\Omega(0)$ decreases if σ_θ increases, $\tilde{\Upsilon}_{\mathrm{P}}(\sigma_\theta)$ turns out to be a decreasing function of σ_θ for high AS values. Consequently, under ideal conditions, in rural and suburban areas, the two designs have the same performance while in urban areas P-DCB outperforms B-DCB. However, under real-world conditions (i.e., accounting for the estimation and quantization errors incurred by each design), from (14), $\tilde{\Upsilon}_{\mathrm{P}}(\sigma_\theta)$ is a decreasing function of $\bar{f}_{\mathrm{D}}$, since $\sigma_{\mathbf{e}_{\mathrm{P}}}^2$ increases with the latter. This means that B-DCB achieves, in rural and suburban areas, an ASANR gain against P-DCB; a gain which increases with $\bar{f}_{\mathrm{D}}$. It also means that in urban environments a higher AS is required to guarantee $\tilde{\Upsilon}_{\mathrm{P}}(\sigma_\theta) < 1$ as $\bar{f}_{\mathrm{D}}$. This results in a wider operational region in terms of AS values over which the B-DCB is favored against P-DCB.

V. PERFORMANCE ANALYSIS IN TERMS OF LINK-LEVEL THROUGHPUT

The problem with the comparisons made above at ASANR level is that they do not factor in the different overhead costs incurred by each design. It is therefore appropriate to make comparisons in terms of the link-level throughput as well. Assuming without loss of generality a BPSK-modulated transmission, the link-level throughput achieved by $\hat{\mathbf{w}}_\star$ is given by [26]

$$\mathcal{T}_{\hat{\mathbf{w}}_\star}(\sigma_\theta) = 0.5\left(R_{\mathrm{T}} - R_{\hat{\mathbf{w}}_\star}^{\mathrm{oh}}\right)\mathrm{E}\{\log_2(1 + \xi_{\hat{\mathbf{w}}_\star})\}, \quad (15)$$

where R_{T} and $R_{\hat{\mathbf{w}}_\star}^{\mathrm{oh}}$ are the transmission bit rate and the overhead bit rate allocated to $\hat{\mathbf{w}}_\star$'s implementation. Obliviously, $\mathcal{T}_{\hat{\mathbf{w}}_\star}(\sigma_\theta)$ is intractable in closed-form which hampers its analytical study. However, the latter can be approximated as [25]

$$\mathcal{T}_{\hat{\mathbf{w}}_\star}(\sigma_\theta) \simeq \tilde{\mathcal{T}}_{\hat{\mathbf{w}}_\star}(\sigma_\theta) = 0.5\left(R_{\mathrm{T}} - R_{\hat{\mathbf{w}}_\star}^{\mathrm{oh}}\right)\log_2\left(1 + \tilde{\xi}_{\hat{\mathbf{w}}_\star}\right). \quad (16)$$

Therefore, the throughput gain given by

$$\mathcal{G}_{\hat{\mathbf{w}}_\star}(\sigma_\theta) = \frac{\tilde{\mathcal{T}}_{\hat{\mathbf{w}}_\star}(\sigma_\theta) - \tilde{\mathcal{T}}_{\hat{\mathbf{w}}_{\mathrm{B}}}(\sigma_\theta)}{\tilde{\mathcal{T}}_{\hat{\mathbf{w}}_{\mathrm{B}}}(\sigma_\theta)}, \quad (17)$$

can be used to compare the CBs' performances. Yet we will shortly see below, both by analysis and simulations, that this simplifying assumption is still able to provide an analytical framework that is extremely insightful qualitatively.

A. Throughput of B-DCB vs. P-DCB

As discussed in Section III-C, P-DCB's implementation requires that the source broadcast all $[\mathbf{h}]_k, k = 1 \ldots K$ for all K terminals. This process requires K time slots of B_{c} bits transmitted at an identification refreshment rate $f_{\mathrm{IR}} = 1/T_{\mathrm{IR}}$

where T_{IR} denotes the refreshment period. It is noteworthy that T_{IR} should satisfy $T_{\mathrm{IR}} \geq T_{\mathrm{c}}$ where $T_{\mathrm{c}} = 0.423/f_{\mathrm{D}}$ is the coherence time and f_{D} is the maximum Doppler frequency. For simplicity, we assume $f_{\mathrm{IR}} = 2f_{\mathrm{D}}$. Therefore, the P-DCB implementation overhead rate is $R_{\hat{\mathbf{w}}_{\mathrm{P}}}^{\mathrm{oh}} = 2B_{\mathrm{c}}f_{\mathrm{D}}$ and, hence, its achieved throughput is

$$\tilde{\mathcal{T}}_{\hat{\mathbf{w}}_{\mathrm{P}}}(\sigma_\theta) = 0.5R_{\mathrm{T}}\left(1 - 2B_{\mathrm{c}}\bar{f}_{\mathrm{D}}\right)\log_2\left(1 + \tilde{\xi}_{\hat{\mathbf{w}}_{\mathrm{P}}}\right). \quad (18)$$

Since when $\bar{f}_{\mathrm{D}}$ increases $\tilde{\xi}_{\hat{\mathbf{w}}_{\mathrm{P}}}$ decreases, it follows then from the above result that $\tilde{\mathcal{T}}_{\hat{\mathbf{w}}_{\mathrm{P}}}$ also decreases if $\bar{f}_{\mathrm{D}}$ increases. Interestingly, from (18), B_{c} has two contradictory effects on $\tilde{\mathcal{T}}_{\hat{\mathbf{w}}_{\mathrm{P}}}$. Indeed, if B_{c} increases the P-DCB overhead rate increases and, hence, $\tilde{\mathcal{T}}_{\hat{\mathbf{w}}_{\mathrm{P}}}$ is decreased. However, as discussed above increasing B_{c} results in improving the ASANR $\tilde{\xi}_{\hat{\mathbf{w}}_{\mathrm{P}}}$ and, therefore, the achieved throughput $\tilde{\mathcal{T}}_{\hat{\mathbf{w}}_{\mathrm{P}}}$ is increased. The result in (18) could then be exploited to find the optimum number of quantization bits $B_{\mathrm{c}}^{\mathrm{opt}}$ that maximizes the throughput achieved using the P-DCB technique.

On the other hand, the B-DCB implementation requires that the source estimates, quantizes and broadcasts ϕ_s and σ_θ. The angular estimate broadcasting requires only one time slot of B_{a} bits transmitted at a localization refreshment rate $f_{\mathrm{LR}} = 1/T_{\mathrm{LR}}$ where T_{LR} is the refreshment period. In turn, the AS estimate broadcasting requires one time slot of B_{s} bits transmitted at an estimation refreshment rate $f_{\mathrm{ER}} = 1/T_{\mathrm{ER}}$ where T_{ER} is the estimation refreshment period. Since T_{LR} and T_{ER} are typically very large compared to T_{IR} (i.e., $T_{\mathrm{LR}} \gg T_{\mathrm{IR}}$ and $T_{\mathrm{ER}} \gg T_{\mathrm{IR}}$), we have both f_{LR} and f_{ER} negligible compared to f_{IR} (i.e., $f_{\mathrm{LR}} \simeq 0$ and $f_{\mathrm{ER}} \simeq 0$), and hence we have $R_{\hat{\mathbf{w}}_{\mathrm{B}}}^{\mathrm{oh}} \simeq 0$. Therefore, the throughput achieved using the B-DCB is

$$\tilde{\mathcal{T}}_{\hat{\mathbf{w}}_{\mathrm{B}}}(\sigma_\theta) \simeq 0.5R_{\mathrm{T}}\log_2\left(1 + \tilde{\xi}_{\hat{\mathbf{w}}_{\mathrm{B}}}\right). \quad (19)$$

As can be shown from (19), in contrast with P-DCB, the B-DCB throughput is independent of the normalized Doppler frequency $\bar{f}_{\mathrm{D}}$ and, therefore, $\mathcal{G}_{\hat{\mathbf{w}}_{\mathrm{P}}}(\sigma_\theta)$ decreases if the latter increases. Furthermore, since we showed in Section IV-B that $\tilde{\xi}_{\hat{\mathbf{w}}_{\mathrm{B}}} \geq \tilde{\xi}_{\hat{\mathbf{w}}_{\mathrm{P}}}$ for high SNR and relatively large B_{a} and B_{s}, we have $\mathcal{G}_{\hat{\mathbf{w}}_{\mathrm{P}}}(\sigma_\theta) < 0$ for large K and low AS. Consequently, the B-DCB outperforms, in rural and suburban areas, its P-DCB vis-a-vis in terms of achieved throughput. Simulations in Section VI will show that this results in a wider operational region in terms of AS values over which the B-DCB is favored against P-DCB. They will also establish that this operation region increases with K and $\bar{f}_{\mathrm{D}}$ and reaches as much as 40 deg for large K and high $\bar{f}_{\mathrm{D}}$, against about 17 deg in ideal conditions (i.e, without accounting for any overhead cost or any quantization or estimation error).

B. Throughput of M-DCB vs. B-DCB

As discussed in Section III-A, the M-DCB implementation only requires that the source estimates, quantizes and broadcasts its angle ϕ_s. Following similar steps as above, it can be easily shown that $R_{\hat{\mathbf{w}}_{\mathrm{M}}}^{\mathrm{oh}} \simeq 0$ and, therefore, $\tilde{\mathcal{T}}_{\hat{\mathbf{w}}_{\mathrm{M}}}(\sigma_\theta) \simeq$
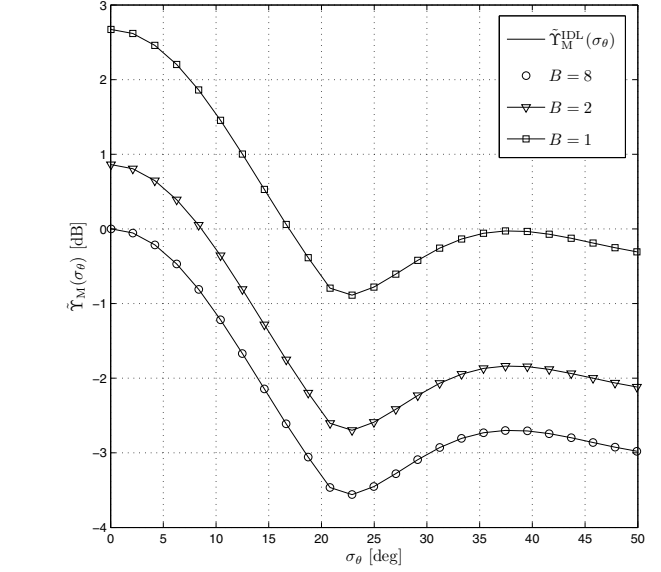
(a) $\tilde{\Upsilon}_{\mathrm{M}}^{\mathrm{IDL}}(\sigma_\theta)$ and $\tilde{\Upsilon}_{\mathrm{M}}(\sigma_\theta)$ for different values of B.
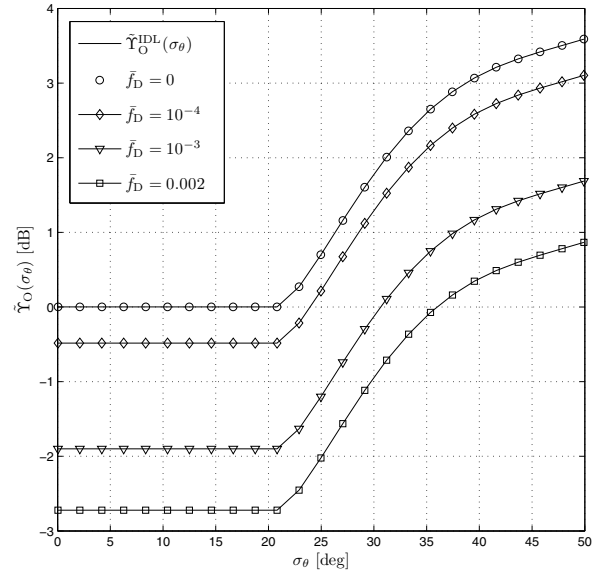
(b) $\tilde{\Upsilon}_{\mathrm{P}}^{\mathrm{IDL}}(\sigma_\theta)$ and $\tilde{\Upsilon}_{\mathrm{P}}(\sigma_\theta)$ for $B = 8$ and different values of $\bar{f}_{\mathrm{D}}$.

Fig. 2. ASANR comparison for $K = 20$ and $B = B_{\mathrm{a}} = B_{\mathrm{s}} = B_{\mathrm{c}}$.

$0.5R_{\mathrm{T}}\log_2\left(1 + \tilde{\xi}_{\hat{\mathbf{w}}_{\mathrm{M}}}\right)$. Thus, we obtain

$$\mathcal{G}_{\hat{\mathbf{w}}_{\mathrm{M}}}(\sigma_\theta) \simeq \frac{\log_2\left(1 + \tilde{\xi}_{\hat{\mathbf{w}}_{\mathrm{M}}}\right)}{\log_2\left(1 + \tilde{\xi}_{\hat{\mathbf{w}}_{\mathrm{B}}}\right)} - 1. \quad (20)$$

Since for reasonable B_{s} and B_{a} $\tilde{\xi}_{\hat{\mathbf{w}}_{\mathrm{M}}} \leq \tilde{\xi}_{\hat{\mathbf{w}}_{\mathrm{B}}}$, we have $\mathcal{G}_{\hat{\mathbf{w}}_{\mathrm{M}}}(\sigma_\theta) \leq 0$, it follows from (20) that the B-DCB is always more efficient than the M-DCB in terms of achieved throughput.

VI. SIMULATION RESULTS

Numerical experiments are performed to verify the analytical results. In all examples, we assume that the noises' powers σ_n^2 and σ_v^2 are 10 dB below the source transmit power. It is also assumed that ϕ_s and σ_θ are estimated using $N = 10$ samples. Furthermore, we assume that the number of rays is $L = 6$ and that their phases are uniformly distributed. All the results are obtained by averaging over 10^6 random realizations of r_k, ψ_k, $[\mathbf{f}]_k$ for $k = 1, \ldots, K$ and α_l, θ_l for $l = 1, \ldots, L$ as well as all the estimation and quantization errors.

Fig. 2(a) displays $\tilde{\Upsilon}_{\mathrm{M}}^{\mathrm{IDL}}(\sigma_\theta)$ and $\tilde{\Upsilon}_{\mathrm{M}}(\sigma_\theta)$ for different values of $B = B_{\mathrm{a}} = B_{\mathrm{s}}$. As can be observed from this figure, for practical value $B = 8$, $\tilde{\Upsilon}_{\mathrm{M}}(\sigma_\theta) \simeq \tilde{\Upsilon}_{\mathrm{M}}^{\mathrm{IDL}}(\sigma_\theta)$. This is expected since for high quantization levels quantization errors are negligible. In such a case, we also show that the B-DCB is much more efficient in terms of achieved ASANR than its M-DCB vis-a-vis. However, from Fig. 2, the achieved ASANR gain using $\hat{\mathbf{w}}_{\mathrm{B}}$ instead of $\hat{\mathbf{w}}_{\mathrm{M}}$ decreases with B. This is expected since $\tilde{\xi}_{\hat{\mathbf{w}}_{\mathrm{B}}}$ is affected by both quantization errors $\mathbf{e}_{\mathrm{aq}}$ and $\mathbf{e}_{\mathrm{sq}}$ while $\tilde{\xi}_{\hat{\mathbf{w}}_{\mathrm{M}}}$ involves only $\mathbf{e}_{\mathrm{aq}}$. Furthermore, it follows from this figure that the M-DCB outperforms the B-DCB only for unrealistic low quantization levels which are hard to justify in practice. This corroborates the discussion made in Section-IV-A.

Fig. 2(b) plots $\tilde{\Upsilon}_{\mathrm{P}}^{\mathrm{IDL}}(\sigma_\theta)$ and $\tilde{\Upsilon}_{\mathrm{P}}(\sigma_\theta)$ for $B = B_{\mathrm{a}} = B_{\mathrm{s}} = B_{\mathrm{c}} = 8$ and different values of $\bar{f}_{\mathrm{D}}$.

From this figure, under ideal conditions, B-DCB and P-DCB achieve the same ASANR, for low AS values, while the latter outperforms the first for high AS values. However, under real-world conditions, the ASANR gain achieved by P-DCB against B-DCB decreases if $\bar{f}_{\mathrm{D}}$ increases. This corroborates the discussion made in Section-IV-B.

Figs. 3(a) and 3(b) plot $\mathcal{G}_{\hat{\mathbf{w}}_{\mathrm{P}}}(\sigma_\theta)$ for different values of $\bar{f}_{\mathrm{D}}$ and B_{c}. They also plot $\mathcal{G}_{\hat{\mathbf{w}}_{\mathrm{P}}}(\sigma_\theta)$ in ideal conditions (i.e, without accounting for any overhead cost or any quantization or estimation error). As can be observed from these figures, in rural and suburban areas where the AS is relatively low, the B-DCB always outperforms the P-DCB in terms of achieved throughput. Their performances become actually equal only in idealistic conditions that ignore the practical effects of both overhead and estimation and quantization errors. Figs. 3(a) and 3(b) also confirm and illustrate the existence of an optimum quantization level $B_{\mathrm{c}}^{\mathrm{opt}}$ that maximizes the throughput (i.e., level that best minimizes combined losses due to errors and overhead) found to be equal to 6 and 5 at $\bar{f}_{\mathrm{D}}$ set to 10^{-4} and 10^{-2}, respectively. At these optimum quantization levels, P-DCB suffers from throughput losses against B-DCB of about 3% and 10%, respectively. The B-DCB's throughput gains against P-DCB indeed increase with higher normalized Doppler frequencies. The operational region in terms of AS values over which the B-DCB is favored against P-DCB also increases from a nominal low AS range of about 17 deg in ideal conditions to about 20 and 25 deg, respectively.

Fig. 4 plot $\mathcal{G}_{\hat{\mathbf{w}}_{\mathrm{P}}}(\sigma_\theta)$ for different values of $\bar{f}_{\mathrm{D}}$. In this figure, curves are plotted after performing a numerical evaluation of
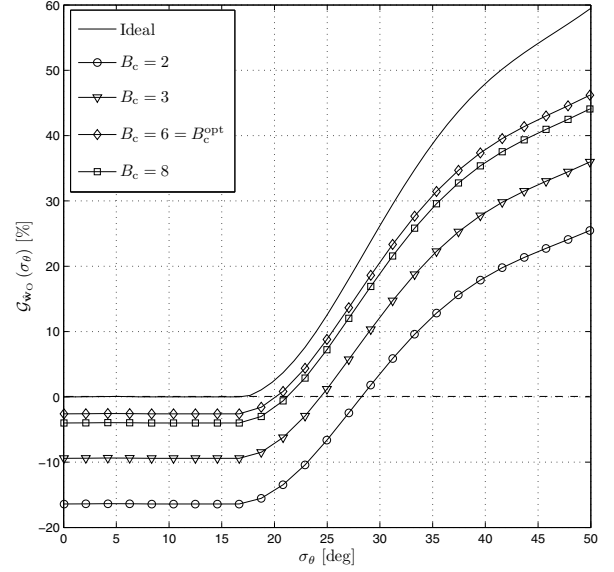
(a) $\bar{f}_{\mathrm{D}} = 10^{-4}$.
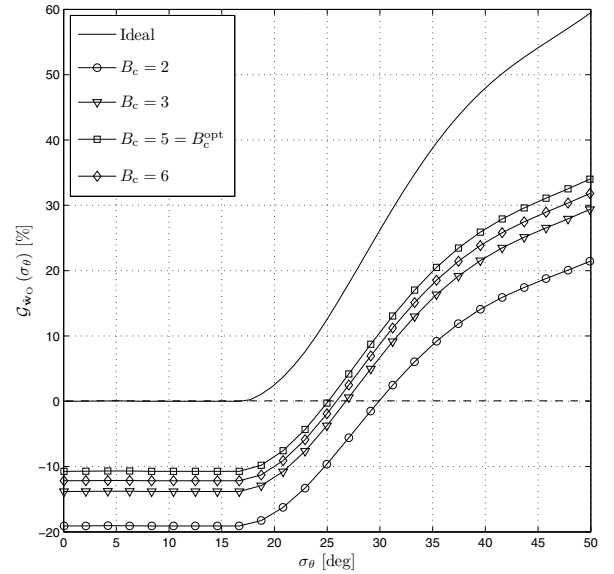
(b) $\bar{f}_{\mathrm{D}} = 10^{-2}$.

Fig. 3. $\mathcal{G}_{\hat{\mathbf{w}}_{\mathrm{P}}}(\sigma_\theta)$ for $K = 20$ and different values of $\bar{f}_{\mathrm{D}}$ and B_{c}.

the optimum quantization level $B_{\mathrm{c}}^{\mathrm{opt}}$ for each values of $\bar{f}_{\mathrm{D}}$. For instance, we find that $B_{\mathrm{c}}^{\mathrm{opt}} = 2$ bits when $\bar{f}_{\mathrm{D}} = 0.002$ while $B_{\mathrm{c}}^{\mathrm{opt}} = 4$ bits when $\bar{f}_{\mathrm{D}} = 10^{-3}$. As can be seen from these figures, the B-DCB's throughput gain against P-DCB increases if $\bar{f}_{\mathrm{D}}$ increases. Furthermore, the B-DCB operational region also increases if $\bar{f}_{\mathrm{D}}$ increases and can reach as much as 40 deg when $\bar{f}_{\mathrm{D}} = 0.002$. All these observations corroborate all the elements of our discussion in Section V-A.

VII. CONCLUSION

In this work, we considered M-DCB, B-DCB, and P-DCB designs to achieve a dual-hop communication from a source
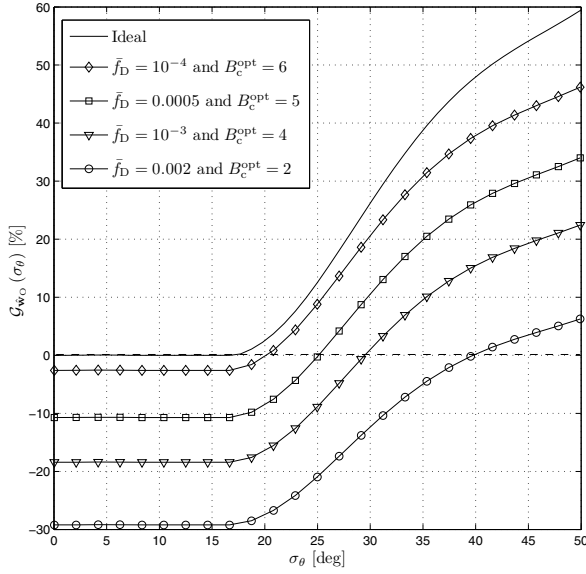
Fig. 4. $\mathcal{G}_{\hat{\mathbf{w}}_P}(\sigma_\theta)$ versus σ_θ for $K = 20$ and different values of $\bar{f}_D$.

to a receiver, through a wireless network comprised of K independent terminals. Assuming the presence of scattering and accounting for estimation and quantization errors incurred by each DCB design, we derived and compared their true achieved ASANR. Excluding exceptional circumstances of unrealistic low quantization levels (i.e., very large quantization errors) hard to justify in practice, we showed that B-DCB always outperforms M-DCB. We also showed that for low AS B-DCB and P-DCB achieve almost the same SNR while for high AS the latter outperforms the first. Furthermore, this work pushed the performance analysis of DCB to the throughput level by taking into account the feedback overhead cost incurred by each design. We proves both by concordant analysis and simulations that the P-DCB's throughput gain against B-DCB reduces as the channel Doppler frequency increases.

REFERENCES

[1] V. Havary-Nassab, S. Shahbazpanahi, A. Grami, and Z.-Q. Luo, "Distributed beamforming for relay networks based on second-order statistics of the channel state information," *IEEE Trans. Signal Process.,* vol. 56, pp. 4306-4316, Sep. 2008.
[2] L. C. Godara, "Application of antenna arrays to mobile communications, Part II: Beam-forming and direction-of-arrival considerations," *Proc. IEEE,* vol. 85, pp. 1195-1245, Aug. 1997.
[3] R. Mudumbai, D. R. Brown, U. Madhow, and H. V. Poor, "Distributed transmit beamforming: challenges and recent progress," *IEEE Commun. Mag.,* vol. 47, pp. 102-110, Feb. 2009.
[4] M. Pun, D. R. Brown III, and H. V. Poor, "Opportunistic collaborative beamforming with one-bit feedback," *IEEE Trans. Wireless Commun.,* vol. 8, pp. 2629-2641, May 2009.
[5] G. Barriac, R. Mudumbai, and U. Madhow, "Distributed beamforming for information transfer in sensor networks," *Proc. 3rd International Workshop Information Processing and Sensor Networks,* 2004.
[6] R. Mudumbai, G. Barriac, and U. Madhow, "On the feasibility of distributed beamforming in wireless networks," *IEEE Trans. Wireless Commun.,* vol. 6, pp. 1754-1763, May 2007.
[7] L. Dong, A. P. Petropulu, and H. V. Poor, "Weighted cross-layer cooperative beamforming for wireless networks," *IEEE Trans. Signal Process.,* vol. 57, pp. 3240-3252, Aug. 2009.
[8] G. Zheng, K.-K. Wong, A. Paulraj, and B. Ottersten, "Collaborative-relay beamforming with perfect CSI: optimum and distributed implementation," *IEEE Signal Process. Lett.,* vol. 16, pp. 257-260, Apr. 2009.
[9] H. Ochiai, P. Mitran, H. V. Poor, and V. Tarokh, "Collaborative beamforming for distributed wireless ad hoc sensor networks," *IEEE Trans. Signal Process.,* vol. 53, pp. 4110-4124, Nov. 2005.
[10] K. Zarifi, A. Ghrayeb, and S. Affes , "Distributed beamforming for wireless sensor networks with improved graph connectivity and energy efficiency," *IEEE Trans. Signal Process.,* vol. 58, pp. 1904-1921, Mar. 2010.
[11] K. Zarifi, S. Zaidi, S. Affes, and A. Ghrayeb, "A distributed amplify-and-forward beamforming technique in wireless sensor networks," *IEEE Trans. Signal Process.,* vol. 59, pp. 3657-3674, Aug. 2011.
[12] K. Zarifi, S. Affes, and A. Ghrayeb, "Collaborative null-steering beamforming for uniformly distributed wireless sensor networks," *IEEE Trans. Signal Process.,* vol. 58, pp. 1889-1903, Mar. 2010.
[13] M. Bengtsson and B. Ottersten, "Low-complexity estimators for distributed sources," *IEEE Trans. Signal Process.,* vol. 48, pp. 2185-2194, Aug. 2000.
[14] A. Amar, "The effect of local scattering on the gain and beamwidth of a collaborative beampattern for wireless sensor networks," *IEEE Trans. Wireless Commun.,* vol. 9, pp. 2730-2736, Sep. 2010.
[15] S. Zaidi and S. Affes, "Distributed collaborative beamforming design for maximized throughput in interfered and scattered environments". Accepted for publication in *IEEE Trans. Commun.,* Oct. 2015.
[16] M. Souden, S. Affes, and J. Benesty, "A two-stage approach to estimate the angles of arrival and the angular spreads of locally scattered sources," *IEEE Trans. Signal Process.,* vol. 56, pp. 1968-1983, May 2008.
[17] S. Zaidi and S. Affes, "Distributed beamforming for wireless sensor networks in local scattering environments" *Proc. IEEE VTC'2012-Fall,* Québec City, Canada, Sep. 3-6, 2012.
[18] S. Zaidi and S. Affes, "Distributed collaborative beamforming in the presence of angular scattering," *IEEE Trans. Commun.,* vol. 62, pp. 1668-1680, May 2014.
[19] S. Zaidi, B. Hmidet, and S. Affes, "Power-Constrained Distributed Implementation of SNR-Optimal Collaborative Beamforming in Highly-Scattered Environments," *IEEE wireless Commun. Lett.,* Vol. 4, pp. 457-460, Oct. 2015.
[20] Y. Jing and H. Jafarkhani, "Network beamforming using relays with perfect channel information," *IEEE Trans. Inf. Theory,* vol. 55, pp. 2499-2517, June 2009.
[21] Y. Zhao, R. Adve, and T. Lim, "Improving amplify-and-forward relay networks: Optimal power allocation versus selection," *IEEE Trans. Wireless Commun.,* vol. 6, pp. 31143123, Aug. 2007.
[22] S. Affes and P. Mermelstein, "Adaptive space-time Processing for wireless CDMA," Chap. 10, pp. 283-321, in *Adaptive Signal Processing: Application to Real-World Problems,* J. Benesty and A. H. Huang, Eds., Springer, Berlin, Germany, Feb. 2003.
[23] A. V. Oppenheim, R. W. Schafer, and J. R. Buck, *Discrete-Time Signal Processing,* 2nd edition Prentice Hall, New Jersey, USA, 1999.
[24] F. Bellili, S. B. Hassen, S. Affes, and A. Stephenne, "Cramer-Rao lower bounds of DOA estimates from square QAM-modulated signals," *IEEE Trans. Signal Process.,* vol. 59, pp. 1675-1685, June 2011.
[25] S. Zaidi and S. Affes, "SNR and throughput analysis of distributed collaborative beamforming in locally-scattered environments," Invited Paper, *Wiley Journal of Wireless Commun. and Mobile Computing,* vol. 12, pp. 1620-1633, 2012.
[26] M. K. Simon and M.-S. Alouini, *Digital Communications over Fading Channels,* Wiley, New York, USA, 2000.